DeDop

Fully Adaptable and Configurable Altimeter Delay Doppler Processor

Sentinel 3 For Science – SAR Altimetry Studies

SEOM Study 1. SARAE

DeDop Case Study Report <Iceberg detection>

WP6100

Project reference: DeDop_ESA_TN_NN

Issue: v.1

24 Jan 2017

Activity: SEOM SARAE

This page has been intentionally left blank

Change Record

Date	Issue	Section	Page	Comment

Control Document

Process	Name	Date
Written by:	Jean Tournadre	24 Jan 2017
Checked by		
Approved by:		

Subject	DeDop Case Study *1*	Project	SARAE (DeDop)

Author	Organisation	Internal references
Jean Tournadre	IFREMER	

	Signature	Date
For DeDop team		
For ESA		

Table of Contents

List of Figures

List of Tables

1 Introduction

1.1 Purpose

Altimeters are powerful tools to detect targets emerging from the sea surface such as icebergs, ships, platforms or small islands (RD.1). Basically, any target emerging from the sea surface gives an echo in the thermal noise part (TNP) of altimeter waveforms if its range lies within the altimeter analysis window and if its backscatter is high enough to come out of the measurement noise. The range depends on the distance from nadir and of the target elevation. The signature is purely deterministic and, for pulse limited altimeter, has a parabolic shape in the waveform space. The method of detection of icebergs has been presented in detail by Tournadre et al, 2008 (RD.2). Under hypotheses on ice backscatter and iceberg freeboard, the iceberg's area can be inferred from the measured backscatter and range (RD.3). A twenty-two year (1992-2014) climatology of the probability of presence, volume of ice and surface based on the analysis of the archives of nine conventional altimeters has been produced within the CNES funded ALTIBERG project (RD.4). This data-set include Cryosat-2 LRM archive.

Cryosat-2 is the first altimeter to operate in three different modes over the ocean. Over most of the open ocean it operates in the classical pulse limited mode and switch to Delay-Doppler Altimeter (DDA) or SAR mode near the sea ice edge, giving a good opportunity to test and validate a method of detection of iceberg using SAR altimeter. Tests have already been conducted on Cryosat-2 data showing that the stacking process used to compute the SAR waveforms significantly reduces the noise level of the waveform thermal noise part used for detection and facilitates the detection especially for smaller icebergs whose backscatters are too low to come out of RDSAR noise. The LRM parabolic signature of icebergs reduces in SAR data to bright spots. They can be easily detected using classical connected components and region properties algorithms (RD.5). The iceberg area can be estimated using the along-track width and across-track length of the signature.

The WP's purpose is to further test the iceberg's detection capabilities and algorithm for Sentinel-3 data, to determine the best processor configuration and to propose a simple algorithm to detect ship/iceberg in Sentinel-3 L1B data.

1.2 Document structure

The first section of this document presents the purpose of the WP, i.e. the demonstration of the improved capacities of SAR altimeter to detect icebergs and ships and to test the DeDop processor configurations to determine the best ones for the detection.

The second section presents the data set used for the case study and the method of detection of icebergs using L1B SAR altimeter data.

The third section presents two case studies of icebergs detection near Greenland and Antarctica. Four DeDop configurations are tested and the results of the detection and of the iceberg area estimates are validated by comparison with the results of the detection and size estimates using Reduced SAR data and MODIS images.

The Fourth section gives some recommendations for the processor's improvements.

1.3 Acronyms

AD	Applicable Document
CC	Connected Component
DDP	Delay-Doppler Processor
DMP	Data Management Plan
ESA	European Space Agency
HRM	High Resolution Mode
ISP	Instrument Source Packet
L1A	Input file with geo-located bursts of Ku echoes. The calibrations are not applied. Each record contains 1 SAR burst of aligned but not-calibrated echoes
L1B-S	Output file with fully processed and calibrated SAR complex echoes, arranged in stacks after slant range correction and prior to echo multi-looking.
L1B	Output file with fully calibrated multi-looked power echoes (SAR)
RD	Reference Document
RDSAR	Reduced SAR echoes or Pseudo-LRM waveforms.
SAR	Synthetic Aperture Radar
TNP	Thermal Noise Part

1.4 References

1.1.1 Applicable Documents

1.1.2 Reference Documents

RD.1	Tournadre, J., Signature of Lighthouses, Ships, and Small Islands in Altimeter Waveforms *J. Atmos. Oceanic Tech., 24*, 1143-1149, 2007,
RD.2	Tournadre J., K. Whitmer, and F. Girard-Ardhuin. Iceberg detection in open water by altimeter waveform analysis. J. Geophys. Res., 113(C8):C08040, 2008
RD.3	Tournadre J, F Girard-Ardhuin, and B Legresy. Antarctic icebergs distributions, 2002-2010. J. Geophys. Res., 117, 2012.
RD.4	Tournadre, J.; Bouhier, N.; Girard-Ardhuin, F. & Remy, F., Antarctic icebergs distributions 1992-2014, *J. Geophys. Res., 121*, 327-349, 2016
RD.5	Gómez-Enri, J.; Scozzari, A.; Soldovieri, F.; Coca, J. & Vignudelli, S. Detection and Characterization of Ship Targets Using CryoSat-2 Altimeter Waveforms *Remote Sensing, 8*, 193, 2016.
RD.6	Dinardo,S., Guidelines for reverting Waveform Power to Sigma Nought for CryoSat-2 in SAR mode, XCRY-GSEG-EOPS-TN-14-0012, ESA,2016
RD.7	Smal I., M. Loog, W. Niessen and E. Meijering, Quantitative Comparison of Spot Detection Methods in Fluorescence Microscopy, *IEEE Transactions on Medical Imaging* 29, 2, 282-301, 2010.

2 Case Study Description

2.1 Scientific / Technical Context

The case study concerns two Cryosat-2 orbits in SAR mode for which icebergs were detected. These two orbits were converted to Sentinel-3 like data and are used to test the iceberg detection algorithm and the method to estimate the iceberg characteristics. As the detection sensitivity strongly depends on the number of samples in the waveform TNP (i.e. above sea level) and on the TNP noise level different processor configurations are tested to determine the best one.

2.2 Objective / Purpose of Case Study

The objective is to demonstrate that SAR altimeter data can detect targets emerging from the sea surface and that SAR processing improves the detection capacities compared to conventional pulse limited altimeter, as it strongly reduces the waveform noise level.

2.3 Input Data Sets (including auxiliary and validation data sets)

Two orbits are used

- CS_LTA__SIR1SAR_FR_20130303T030418_20130303T030503_C001.DBL

- CS_OFFL_SIR1SAR_FR_20150710T233640_20150710T233811_C001.DBL

One near Antarctica and one near Greenland.

Both L1B and L1BS data are used.

One MODIS image is used to validate the iceberg detection;

- MYD02QKM.A2015191.1740.006.2015192153128.hdf (source NASA)

2.4 DeDop Tool Processing Specifications and Description

Four configurations are used to test mainly the impact of zero padding and hamming filtering on the noise level of the TNP of waveforms

1. Default
2. Default, no zero padding
3. Default zero padding, hamming filtering
4. Default, no zero padding, hamming filtering

2.5 Additional Post DeDop Processing

The incoherent summation of the L1B-S to produce the SAR echoes reduces the icebergs LRM parabolic signatures to bright spots. These kind of signatures were also observed for ships and validated using Automatic Identification System data (RD.5) Several image processing algorithms exist to detect bright spots within images. They are generally based on noise reduction, signal enhancement and signal thresholding to create a binary image in which connected components (CC) are detected (see for example RD.7).

The L1B and L1B-S data produced by the DeDop processor are then used to detect icebergs. Figure 1 presents the block diagram of the detection algorithm.

- Selection of the waveforms over sea ice free ocean
- Computation of the mean waveform ($\overline{WF}$) and rms (σ_{WF}) computed from the sea ice free waveforms.
- Normalization of the waveforms:$WF'(i,j) = \frac{\left(WF(i,j)-\overline{WF}(j)\right)}{\sigma_{WF}}(j)$
- Creation of binary image d by thresholding WF' at 4 (i.e. four times the rms of the signal).
- Determination of the binary image connected components using classical graph theory algorithms such as Matlab *bwconncomp* or SCiPy *label* routines.
- Computation of CC's properties; area, position, mean and maximum backscatter using Matlab or SCiPy *regionprops* routines.

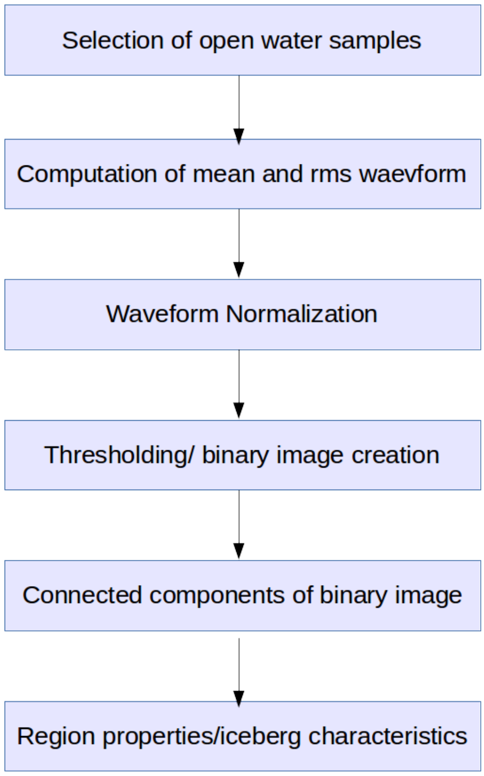

Figure 1: Post-Processing, Iceberg detection algorithm

3 Analysis of Case Study Output

3.1 Technical / Scientific Results

3.1.1 CASE 1 Icebergs near Greenland

Figure 2 presents the MODIS image 6 hours before the CRYOSAT-2 pass on July 10th 2015. Two icebergs are clearly visible near 74°54'N and 75°00N.

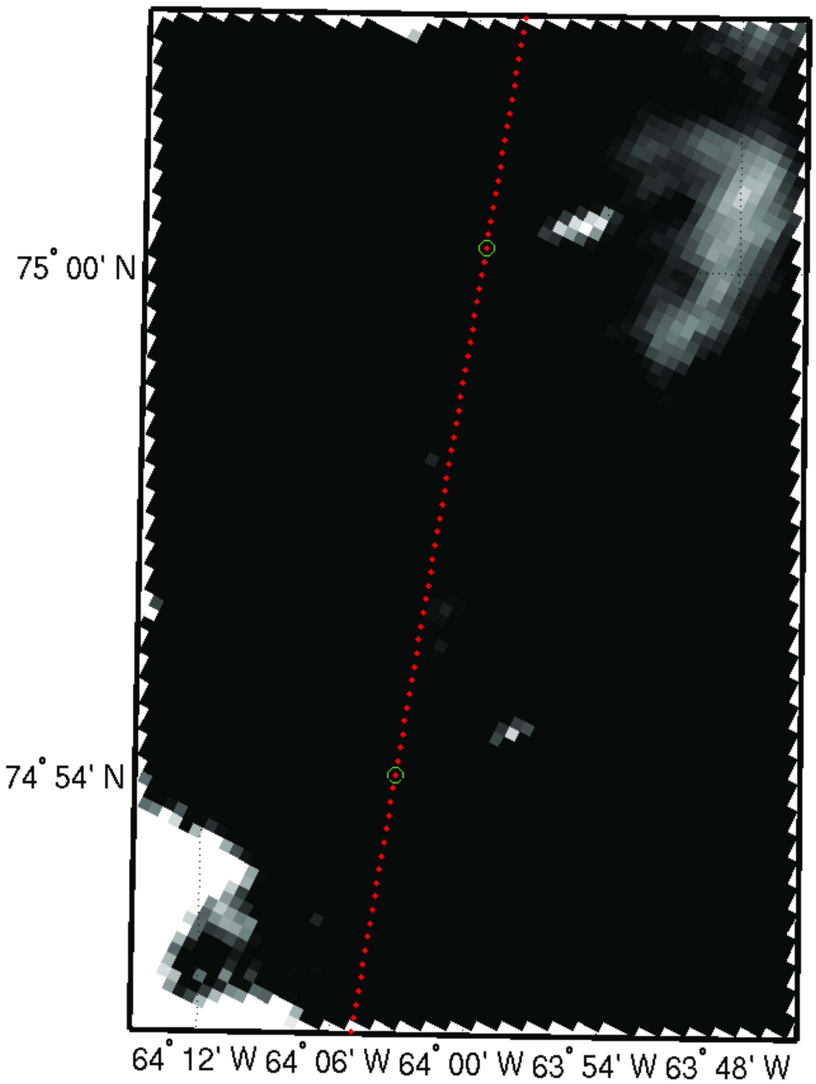

Figure 2: MODIS visible image on July 10th 2015 17:40 UT. The Cryosat-2 (July 10th 2015 23:33UT) satellite ground track is presented as a red line.

Figure 3 presents the waveforms TNP of RDSAR data (computed from the Delay Doppler maps of L1A data) and the SAR echoes TNP for the four different processor configurations. The waveform energy has been rescaled to take into account the zero padding and hamming filtering using the formulas presented in RD.6. The two icebergs have the classical parabolic shape signatures in the pseudo-LRM RDSAR waveforms. It should be note that a secondary lighter parabola is also associated to each iceberg. They correspond to different elevations and/or portions of the icebergs. For SAR echoes iceberg signatures reduce to bright spots for the 4 processor's configurations. Several bright spots are associated to each iceberg corresponding to different freeboard elevations. The icebergs detected in RDSAR using the classical parabola detection algorithm (RD.2) are presented in the figure as black stars while the ones detected using the algorithm of section 2.5 are presented as red circles. The comparison of the two algorithm shows that the two icebergs are detected by both methods and for the four configurations.

However, the noise reduction brought by SAR processing allows the detection of a third small iceberg at 74.9°N that could be detected in RDSAR. A light parabola can be seen in the data but the backscatter is not high enough to come out of the noise.

The use of zero padding doubles the number of waveform samples and increase the size in pixel of the iceberg signature. It thus allows a better detection and a finer description of the icebergs signature.

The hamming filtering strongly reduces the noise level of the waveforms TNP and further improves the detection, especially near the leading edge of the waveforms where the noise reduction is larger.

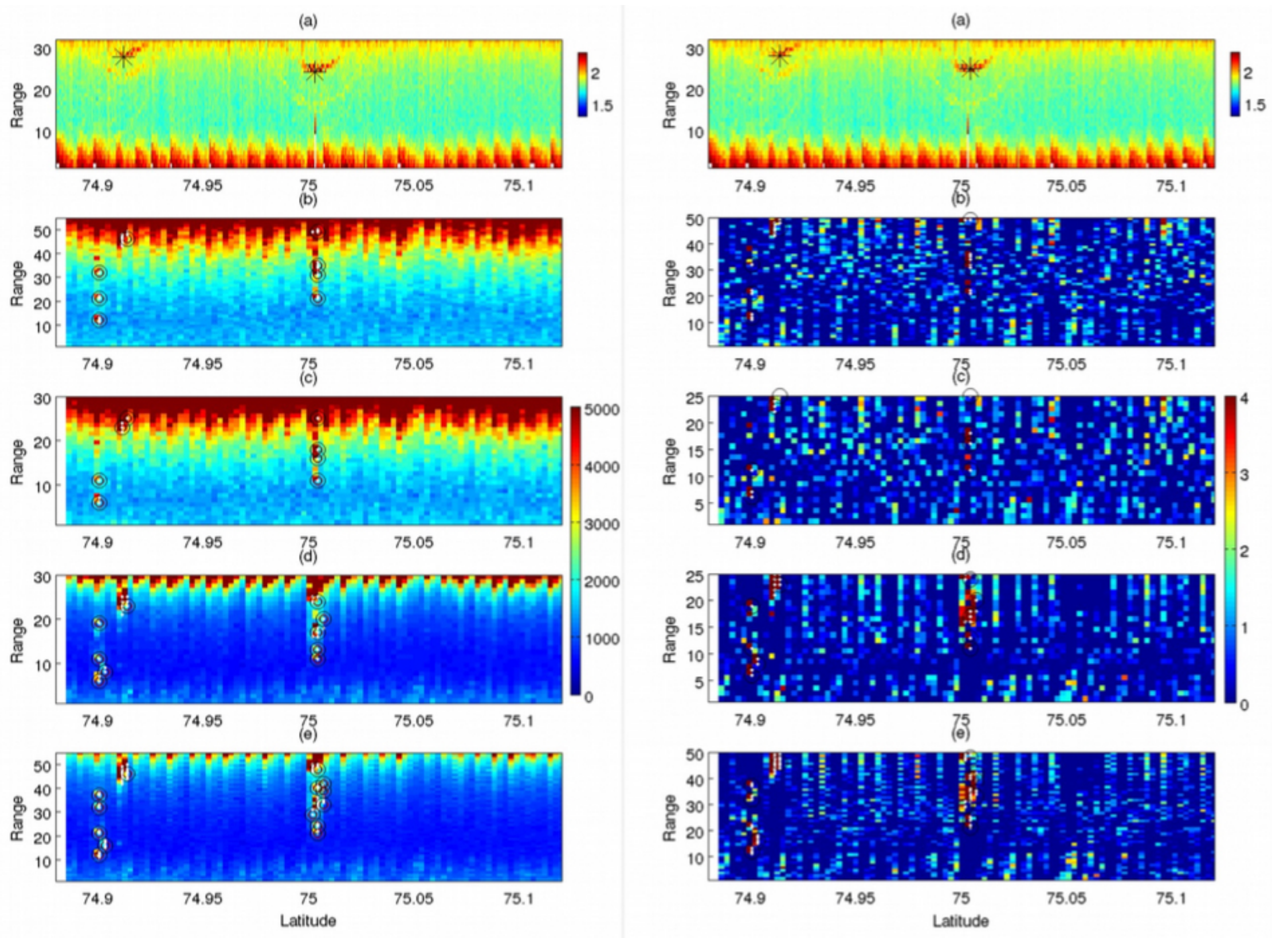

Figure 3 The Cryosat-2 (July 10th 2015 23:33UT) waveforms. LEFT (a) Reduced (LRM like) SAR waveforms, showing the parabolic signatures of the two icebergs. (b) (c) (d) and (e) SAR echoes for processor configurations 1 to 4. In SAR echoes the icebergs signatures reduce to bright spots. RIGHT, same as left but the SAR echoes are the normalized ones used for the detection. The red circles represent the SAR detected icebergs. The black stars represent the icebergs detected in RDSAR.

Figure 4 presents the mean ($\overline{WF}$) waveforms and rms (σ_{WF}) for the 4 configurations. As for Figure 5 the waveform energy has been rescaled to into account the zero padding and hamming filtering using the formulas presented in RD.6. The use of zero padding does not significantly modify the noise level and rms while hamming filtering strongly reduces the mean noise and reduces the rms.

The normalized waveforms used for detection also presented in Figure 6 confirm the noise level reduction by hamming filtering.

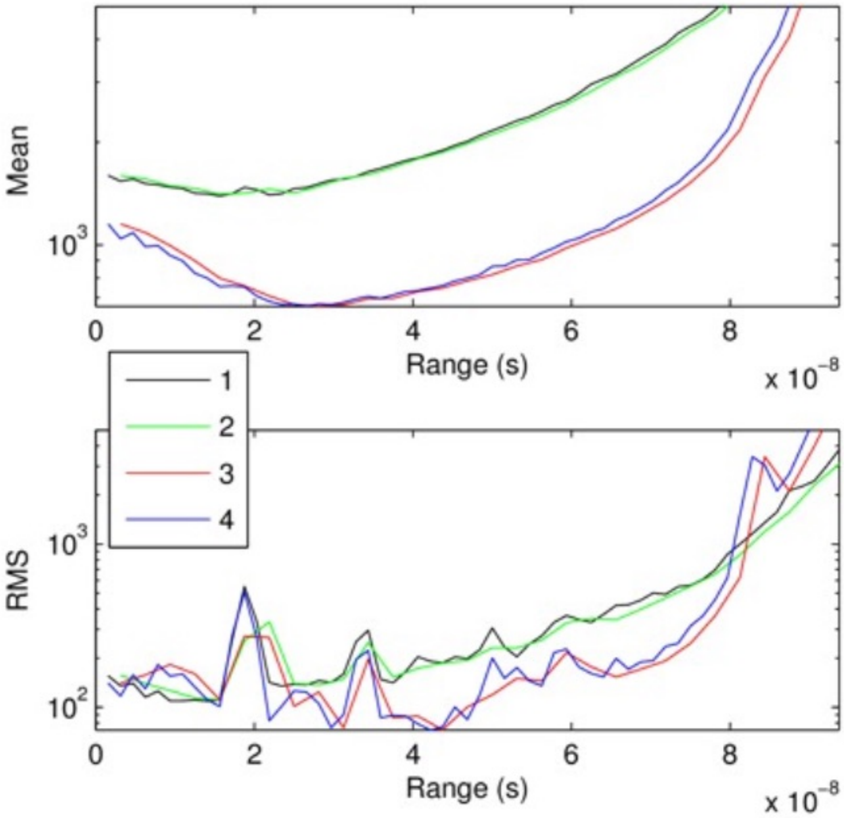

Figure 4: Mean and RMS of waveforms for the 4 configurations

To illustrate the signature of icebergs within stacked data, Figure 5 presents L1B-S data for the largest iceberg at 75.0°N and for the smallest one at 74.9°N. Within L1B-S data stacking and multi-looking processes correct the range within the Delay Doppler Map and co-locates the Doppler beams from different bursts. The signature of an iceberg within L1B-S should therefore be a bright line of constant range and backscatter. Such lines can be easily seen in the figure. However, the specularity of ice backscatter and the antenna beam pattern strongly modulate the backscatter limits the signature to small incidences.

The figure clearly shows the noise reduction by Hamming filtering and that the reduction is stronger at higher incidence.

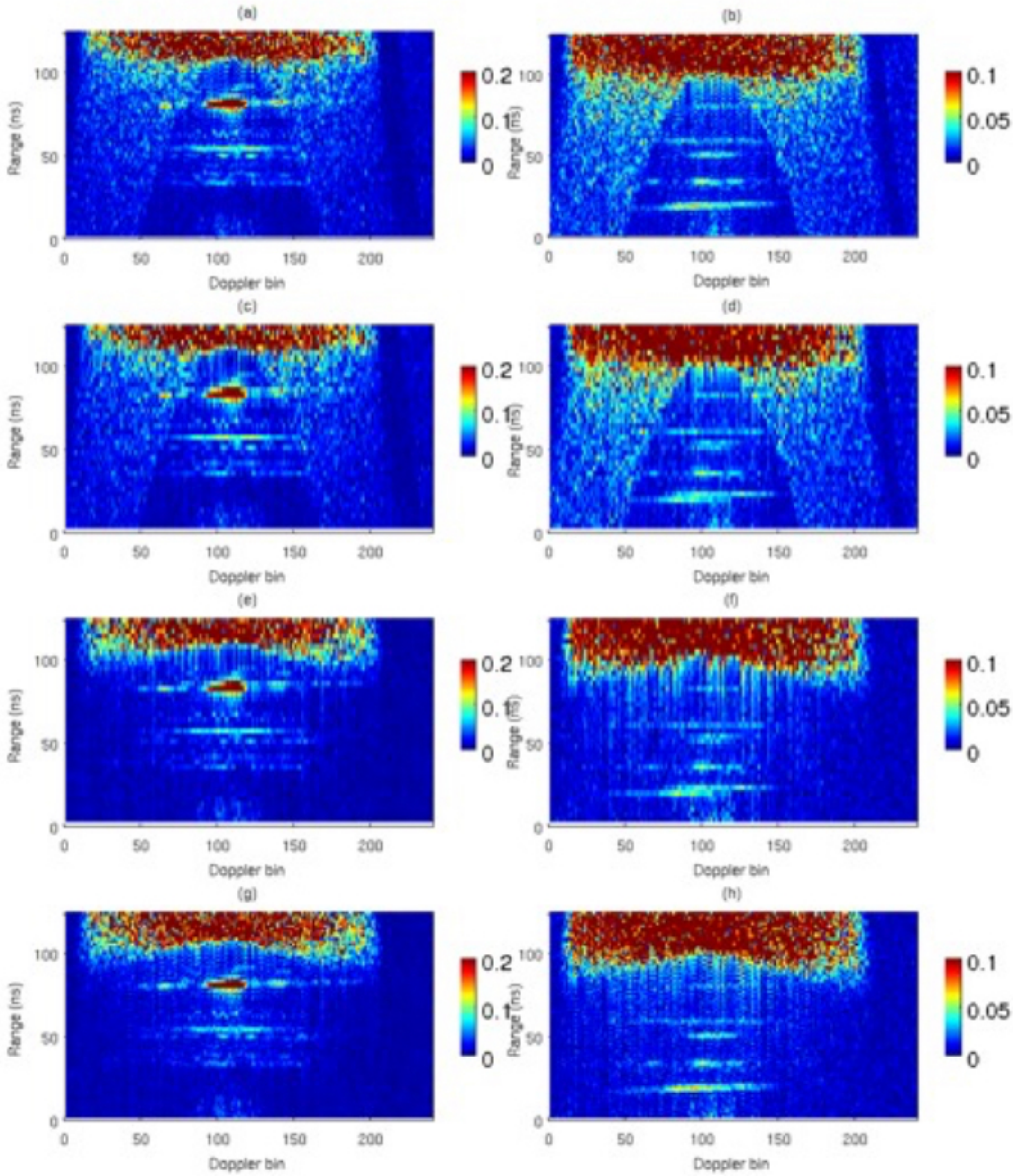

Figure 5: Stacked data for the two main icebergs and for the different configurations. (a-c-e-g) near 75,0°N configurations 1 to 4. (b-d-f-h) near 74.9°N configurations 1 to 4.

The detection algorithm relies on the computation of the connected components of the binary image obtained by thresholding the normalized waveforms. The characteristics of the CC's presented in figure 5 are given in Table 1. For configurations 1 and 4 the pixel size has been divided by 2 to take into account the zero padding. The comparison of the configurations shows that Hamming filtering allows a better estimate of the signature and a better discrimination between the different echoes from the same icebergs. While zero padding appears to have a very limited impact on the detection in absence of filtering, the combined use of zero padding and filtering greatly improves the detection.

Table 1: Connected Components of the detected icebergs for the four configurations

config	1			2			3			4		
	Latitude	*Area pixel*	*Backscatter dB*	*Latitude*	*Area pixel*	*Backscatter dB*	*Latitude*	*Area pixel*	*Backscatter dB*	*Latitude*	*Area pixel*	*Backscatter dB*
Iceberg 1	75.0	1	36.7	75.0	1	36.6	75.0	5	36.3	75.0	5	36.2
	75.0	1	37.9	75.0	1	37.3	75.0	1	33.7	75.0	0.5	33.7
	75.0	1.5	40.0	75.0	1	41.4	75.0	1	34.9	75.0	0.5	34.1
	75.0	1	40.2	75.0	1	40.5	75.0	1	33.9	75.0	1	35.1
							75.0	1	39.1	75.0	1	33.8
										75.01	1	35.1
										75.01	1	39/3
										75.01	3	31.4
Iceberg 2	74.9	1.5	36.8	74.9	2	35.9	74.9	1	34.1	74.9	1	36.2
	74.9	1	35.8	74.9	1	35.4	74.9	2	34.3	74.9	1	34.4
	74.9	0.5	36.1							74.9	1	33.5
										74.9	1.5	34.3
Iceberg 3	74.91	4	39.7	74.91	1	39.0	74.91	2	37.7	74.91	7.5	38.1
				74.91	3	39.8	74.91	2	32.3	74.91	2	32.3

The area of icebergs 1 and 2 have been estimated at 1.1 and 0.26 km^2 using the RD.3 method to infer the iceberg area from its backscatter and range. Due to the quite low resolution of MODIS images (250 m) and the difficulty to precisely delineate the icebergs only crude estimates of the area of the icebergs can be made. The analysis of the images gives 0.6-1 km^2 and 0.3-0.4 km^2 for the two icebergs in good agreement with the RDSAR values. The area of the icebergs is estimated from the SAR area signature. The length of the iceberg in range, l_y , is assumed to extent from the minimum to the maximum range value of the detected CC at the same along-track location while the width, w_x , is the along-track width at a 300 m resolution. The area of the iceberg is thus

$$A_i = w_x dx l_y dy 1$$

where dx and dy are the along and across-track resolutions. The across-track resolution depends of the freeboard elevation and distance from nadir of the icebergs. For distance from nadir between 2 and 7 km, dy varies from $\approx$ 75 to $\approx$ 20 m. These limits are used to estimate the iceberg's area.

Table 2 compares the different area estimates for the four configurations. Zero padding and filtering gives area estimates the closest to the RDSAR and MODIS ones.

Table 2: Iceberg's area estimate in km^2

	Conf 1	Conf2	Conf 3	Conf4	RDSAR	MODIS
Iceberg 1	0.5-0.8	0.3-0.4	0.6-0.8	0.9-1.3	1.1	0.6-1.0
Iceberg2	0.1-0.2	01-0.2	0.25-0.36	0.17-0.24	0.3	0.3-0.4
Iceberg3	0.2-0.3	0.1-0.15	0.3-0.4	0.3-0.4	-	-

3.1.2 CASE 2 icebergs near Antarctica;

The second test case concerns a Cryosat-2 pass near Antarctica where several icebergs were detected using the RDSAR data, near 70°S, 69.5°S, 68.5°S 68.2°S and 68.1°S (Figure 6). For the main icebergs SAR data give the same detection results as the RDSAR. Zero padding and filtering, as it can be seen in the figure, bring the same detection improvements as in Case 1. In particular zero padding allows the detection a very small iceberg near 69.75°S. A close examination of the RDSAR shows a very weak parabolic signature at this location. Filtering further allows the detection of an iceberg close to the leading edge near 68.7°S that did not come out of the noise of non-filtered data.

The two very large parabolas clearly visible near 70°S and 69.5°S that extend beyond the analysis window are not detected using zero padding and filtering or badly positioned. These signatures correspond to icebergs whose range (related to their freeboard and distance to nadir) lie outside the nominal analysis window. However, a test conducted using the SARVATORE processor, in particular its extended window analysis option (see figure 7), shows that extending the window analysis above the sea level can strongly increase the swath over which the detection is possible. The two large parabolas are associated to 2 large icebergs whose freeboard elevations is at least 28 high.

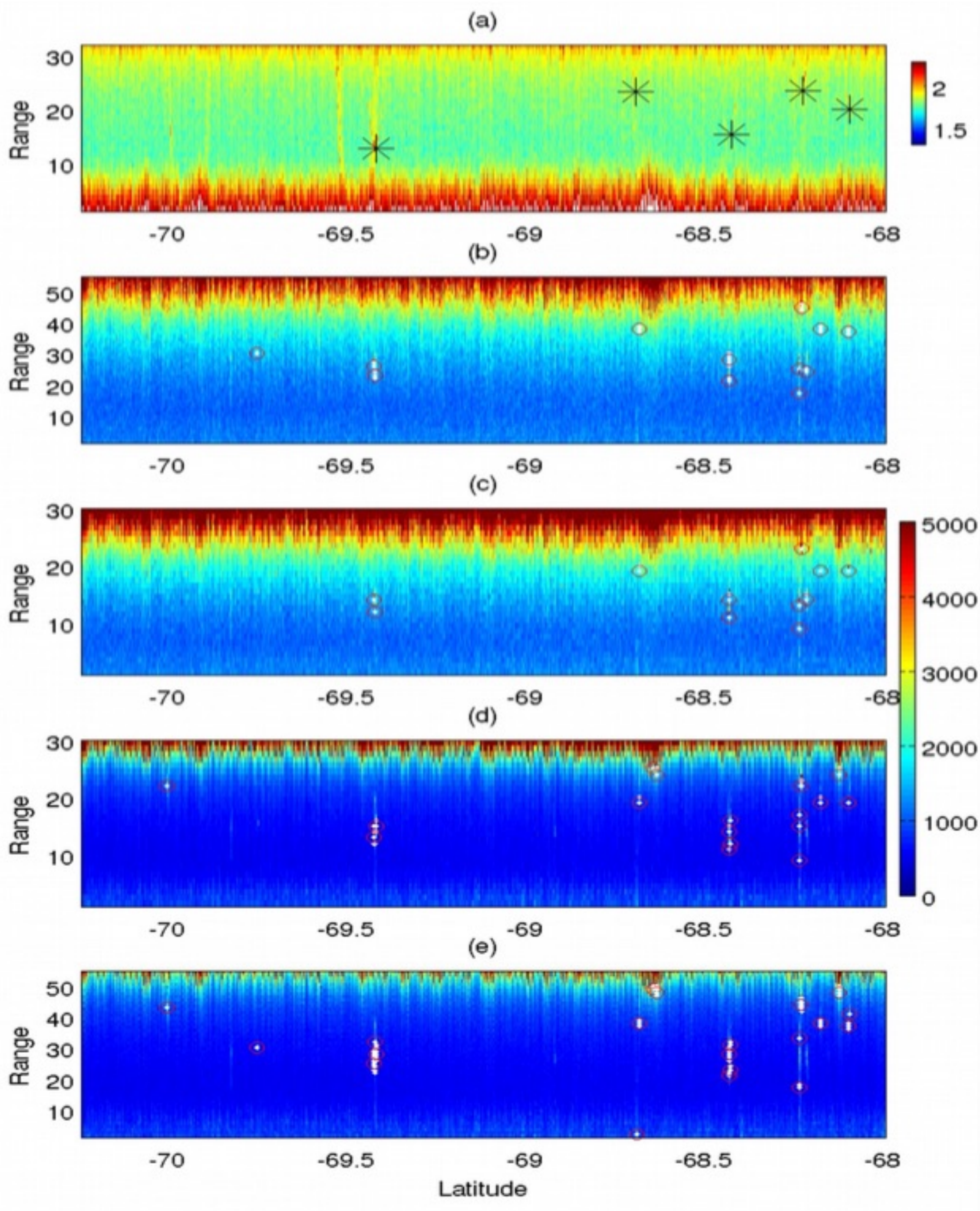

Figure 6: The Cryosat-2 (March 3 2013 030:41UT) waveforms. (a) Reduced (LRM like) SAR waveforms, showing the parabolic signatures of the two icebergs. (b) (c) (d) and (e) SAR echoes for processor configurations 1 to 4. The red circles represent the SAR detected icebergs. The black stars represent the icebergs detected in RDSAR.

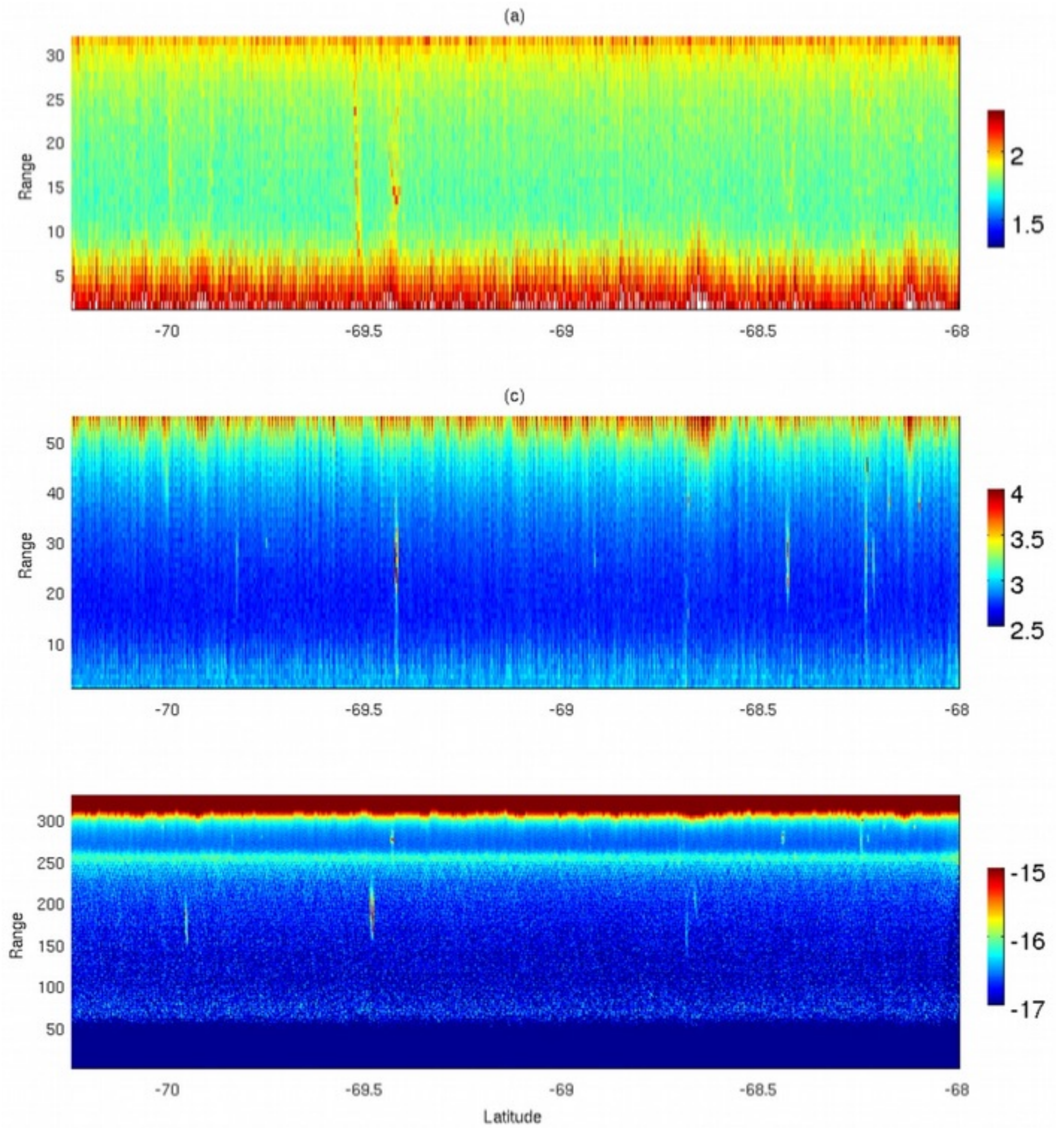

Figure 7: Thermal noise part of the RDSAR (a), SAR configuration 4 (b), extended analysis window SARVATORE (c) waveforms.

3.2 Impact of Different DeDop Processing Configurations

For iceberg and ship detection, only the Thermal Noise Part of the waveforms is considered. Only the parameters that directly impact the TNP noise level and the number of range bins available can significantly modify the detection and the icebergs parameters estimates. Zero padding doubles the numbers of range bins and thus increases the size of the iceberg's signature allowing a more precise estimate of their size. Hamming filtering strongly reduces the TNP noise level and allows a better detection of smaller iceberg whose backscatter is low and decreases the probability of false alarm.

3.3 Product Validation Report

The two case studies were chosen because they had already been processed using the standard Cryosat 2 L1A and L1B data. Using the SARVATORE processor, the four processing configurations had been tested for icebergs detection. The DeDop processor allows producing identical results for iceberg detection. The results are so similar that the figures are identical to the ones presented. The only difference results from the possibility using SARVATORE to extend the analysis window and thus to increase the swath the swath over which icebergs can be detected.

3.4 DeDop Processor and Tool Performance

The processor performs well but quite slowly. Further improvements should include the capacities to produce 80Hz L1BS data and to extent the processing window when stacking, i.e. to allow the leading edge to move to the center of analysis window to extent the TNP. This was possible in the SARVATORE processor.

4 Conclusions/Recommendations

Sentinel-3 L1B data are powerful tools to detect icebergs and ships. The comparison with RDSAR, i.e. data equivalent to classical pulse limited altimeter data shows that SAR processing improves the detection; The comparison of the different DeDop processor configurations shows that both zero padding and Hamming filtering improves the detection and the icebergs area estimates by increasing the number of range bins available for the detection and by reducing the noise of the waveforms TNP.

Tests that have been conducted using Cryosat-2 data and the ESA SARVATORE processors show that the detection could be further improved by extending the analysis window during the stacking process. Indeed the swath over which icebergs can be detected could be doubled.

End of the document